Resonant charge transfer in grazing scattering of alkali-metal ions from an Al(111) surface

A. G. Borisov, D. Teillet-Billy, and J. P. Gauyacq

Laboratoire des Collisions Atomiques et Moléculaires (Unité de Recherche associée au CNRS D0281), Bâtiment 351,
Université Paris-Sud, 91405 Orsay Cedex, France

H. Winter and G. Dierkes

Institut für Physik der Humboldt-Universität zu Berlin, Invalidenstrasse 110, D-10115 Berlin, Germany

The nonperturbative coupled-angular-mode (CAM) method is applied to the treatment of the parallel velocity-assisted charge-transfer process in grazing scattering of alkali-metal ions at Al(111) surface. The neutralization of Na^+, K^+, and Li^+ projectiles is studied. A multistate treatment of the problem including projectile ground and excited states is performed. Calculated neutral fractions in the scattered beam agree on a quantitative level with available experimental results over a wide range of scattering conditions. The role of the population of excited states is discussed. [S0163-1829(96)06948-2]

I. INTRODUCTION

Quite a few experimental studies have been performed over recent years on charge exchange between atoms and metal surfaces under a grazing angle of incidence.[1–6] Grazing scattering conditions are characterized by a small velocity component normal to the surface ($v_\perp$), allowing an almost elastic scattering from the topmost layer of the surface atoms. On the other hand, the velocity component parallel to the surface ($\mathbf{v}_\parallel$) is large. Care should then be taken with respect to the fact that electronic states of the atomic particle and the surface are defined in two different reference frames moving one with respect to the other. Clearly, translational factors arising from the transformation from one frame to the other[7,8] affect electronic transitions between the atomic particle and the surface.

A pronounced effect of the collision velocity on the charge states of the scattered particles was observed experimentally for the neutralization of alkali-metal ions as well as for the formation of H^- ions in grazing scattering from metal surfaces.[5,6] Results of those studies have been explained via kinematically affected resonant exchange processes.[5,9–11] Already early perturbative treatments including translational factors associated with $\mathbf{v}_\parallel$ were able to reproduce gross features of the experimental results.[5,12]

Recently nonperturbative methods were applied to obtain the properties of atomic particles in front of metal surfaces.[13–16] Those methods provided quantitative tools to study charge-transfer processes.

In this paper we present a theoretical study of alkali-metal ion neutralization in grazing scattering from a metal surface performed with the nonperturbative coupled-angular-mode (CAM) method.[15] We use the Al(111) target as a prototype of the free-electron metal well described within the "jellium" approximation.[17] Alkali-metal atoms are prototypes for systems with one active electron. Because of their low binding energies, formation of the ground and excited states of the alkali-metal atoms proceeds via resonant electron transfer. Auger capture and Auger deexcitation processes can

be neglected for these systems.[18,19] Experimental studies revealed two different types of $\mathbf{v}_\parallel$ dependence of the neutralization probability: the case of K projectiles was found to be qualitatively different from that of Li and Na projectiles.[5] This makes alkali-metal atoms interesting systems to study, since one can thus treat in the same way different parallel velocity dependences of the neutralization process. Apart from the formation of ground-state atoms, non-negligible fractions of excited atoms in the scattered beam are also formed. Formation of the excited states manifests itself in the photon emission as studied experimentally and theoretically.[4,20–29]

The paper is arranged in the following way. First, we report on the results of static studies of the properties of alkali-metal atom states in front of a metal surface. Those results are used as inputs for the dynamical treatment of the charge-state evolution during grazing collisions. This dynamical treatment is based on a multistate rate equation approach[30,31] where parallel velocity effects are included via the "shifted Fermi sphere" model.[9,10] We consider in our treatment the ground and the first excited states of alkali-metal atoms. Population of higher excited states has been shown to be negligible.[29] Finally we compare the results of our calculations with available experimental data.

II. STATIC PROPERTIES OF ALKALI-METAL ATOMS IN FRONT OF AN Al(111) SURFACE

A. Theoretical method

Details on the CAM method can be found elsewhere.[15,32] We will give only a brief summary here. The method considers the electron scattering in the compound potential V created by the ion-core and the metal surface. Quasistationary atomic states appear as scattering resonances. The energies and widths of the atomic states coupled to the metal surface are associated with the energies and widths of those resonances. The effective potential V consists of three terms:[32]
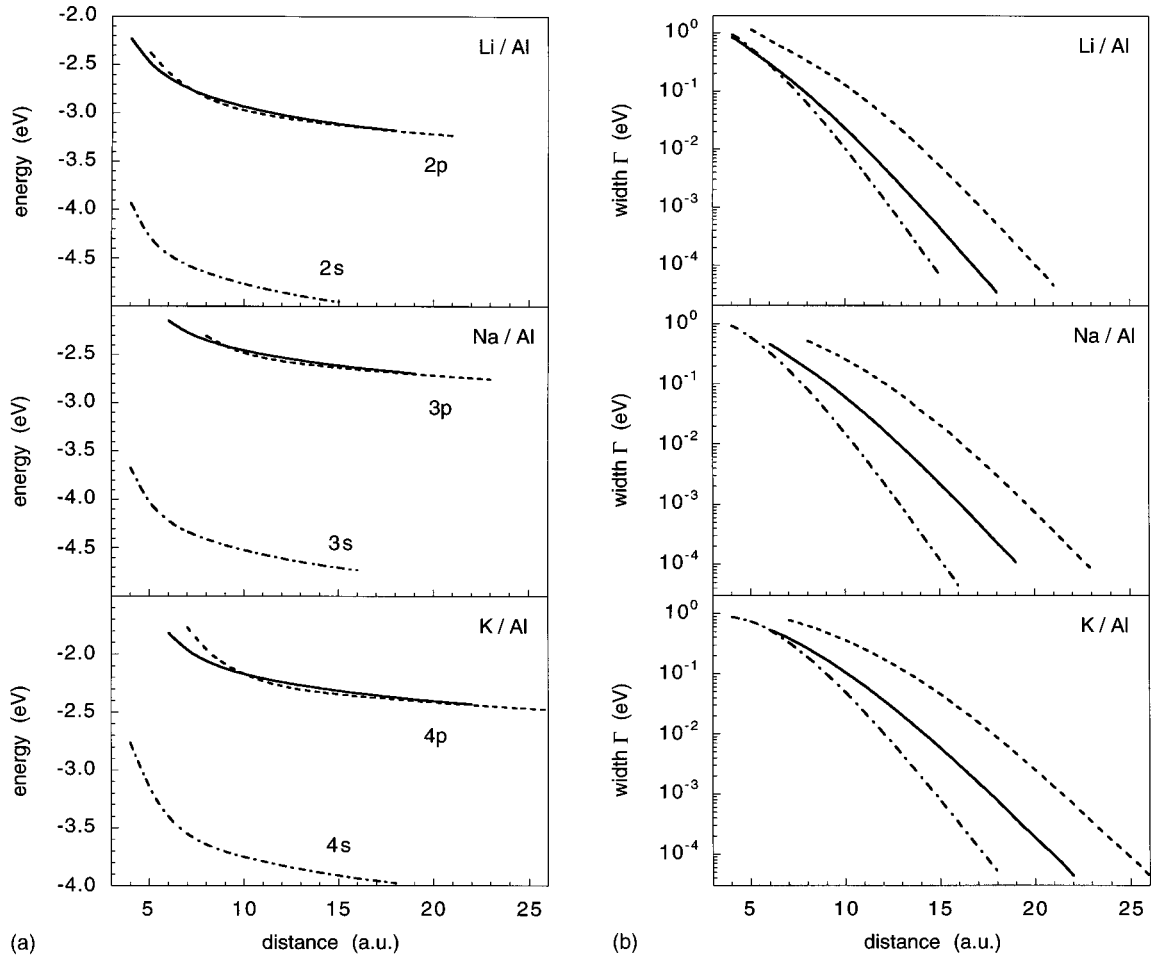
FIG. 1. (a) Energies of the ground and first excited states of the alkali-metal atoms in front of the Al(111) surface as functions of the atom-surface distance measured from the image reference plane. Ground state, dashed-dotted line; $p(m=0)$ state, dashed line; $p(m=\pm 1)$ states, solid line. (b) Widths of the ground and first excited states of the alkali-metal atoms in front of the Al(111) surface as functions of the atom-surface distance measured from the image reference plane. For further details see (a).

$$V=V_{e\text{-core}}+V_{e\text{-metal}}+\Delta V_{e\text{-metal}}. \qquad (1)$$

$V_{e\text{-core}}$=electron interaction with the alkali-metal ion core. It is described by a pseudopotential given by Bardsley.[33] For the electron-metal interaction ($V_{e\text{-metal}}$) we use a potential proposed by Jones et $al.$[34,35] It is constant in the bulk ("jellium" approach with a Fermi energy $E_F=11.65$ eV, and work function W, as measured experimentally) and merges asymptotically to the classical image potential in vacuum. $\Delta V_{e\text{ metal}}$ represents the potential due to response of the metal to the presence of the ion core. It is modeled by a static image charge. In grazing scattering collisions, rather large atom-surface distances Z (measured from the image plane) are important for the final charge state formation ("freezing distance" concept[30]). Therefore our modeling of the potential should hold well. In case small Z contribute to the final charge-state formation, care should be taken to properly modeled surface response.[14,36]

B. Results of the static treatment

Close to the surface, atomic orbitals are modified by the surface potential. As a result, mixtures between, e.g., ns and np orbitals occur ($n=2,3,4$ for Li, Na, and K, respectively).

For continuity we will use an assignment of the orbitals corresponding to the limit at infinite atom-surface separations. This is further supported by the smallness of $v_\perp$, so one can neglect nonadiabatic transitions due to the motion normal to the surface.

Results for the energies (E) and widths (Γ) of Li, Na, and K ground and first excited states are presented in Figs. 1(a) and 1(b). The presence of the surface partly removes the degeneracy of the $m=0$, 1, and -1 magnetic sublevels of the excited Li($2p$), Na($3p$), and K($4p$) states. m is the projection of the angular momentum on the quantization z axis. We choose a z axis normal to the surface going through the atom center to keep the cylindrical symmetry of the problem. $np(m=0)$ and $np(|m|=1)$ orbitals are oriented differently with respect to the surface, so a $priori$ they will have different energies and widths. $m=1$ and -1 substates remain degenerate because of the symmetry. As it is seen in Fig. 1(b), the $np(m=0)$ orbital being oriented towards the surface is more strongly coupled to the metal states and has a width Γ much larger than that of the $np(|m|=1)$ orbitals, lying in the plane parallel to the surface. The ground state has a width much smaller than that of excited states, because of a more localized wave function and, correspondingly, less coupling
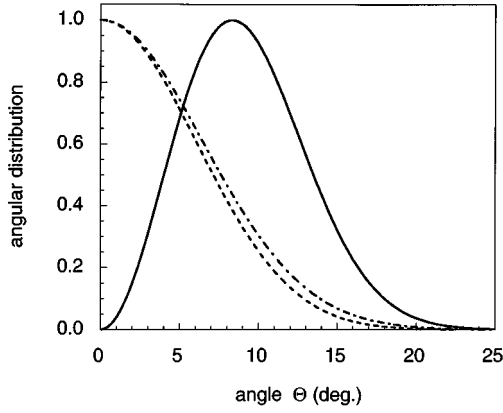
FIG. 2. Angular distributions (normalized to 1 at maximum) for K states in front of the Al(111) surface. Ground state, dashed-dotted line; $p(m=0)$ state, dashed line; $p(m=\pm1)$ states, solid line. The atom-surface distance is 18 a.u.

to the metal states. In first order, all the widths show an exponential dependence on Z except for small Z, where tendency to saturation occurs. Energy shifts of the states in front of the surface can roughly be described by the $1/4Z$ dependence. Deviations from this can be attributed to the van der Waals interaction.[17,37] We should point out that our results are in good agreement with the results of the complex scaling calculations for these systems.[13,14]

Apart from the energies and widths of the states, the CAM method allows us to calculate the angular distributions for the transition probability $|\sigma(\theta,Z)|^2$.[11,32] It is an internal property of the charge transfer and gives the probability of the electron transition between the atomic orbital and metal $|\mathbf{k}\rangle$ orbitals with wave vector $\mathbf{k}$ oriented at an angle θ with respect to the surface normal. Because of the cylindrical symmetry the angular distributions are not dependent on the φ angle. In Fig. 2 we give an example of the angular distributions for the $4s$, $4p(m=0)$, and $4p(|m|=1)$ orbitals of K atom at an atom-surface distance of 18 a.u. As it is seen on the figure, the $4p(|m|=1)$ orbitals have an angular distribution notably different from the other two. This reflects the structure of the $4p(|m|=1)$ orbitals with a zero of the wave function in the $\theta=0$ direction.

III. DYNAMICS OF THE CHARGE EXCHANGE BETWEEN ALKALI-METAL ATOMS AND AN Al SURFACE

A. Transformation of the static results

For grazing scattering experiments the only symmetry of the problem is the symmetry with respect to the scattering plane. This plane is normal to the surface plane and contains the velocity vector [we define it as the (x,z) plane]. Therefore, results obtained by the CAM method within the $|m\rangle$ basis should be transformed into the basis of symmetric and antisymmetric orbitals with respect to the (x,z) plane. As we will see below, the treatment of the dynamical charge transfer by the ''shifted Fermi sphere'' model breaks the cylindrical symmetry around the z axis so that new symmetry-adapted states have to be considered. Obviously this transformation does not concern ns and $np(m=0)$ orbitals

which are symmetric with respect to the scattering plane. The new, symmetry-adapted basis can be constructed as following:

$$|ns\rangle,$$

$$|np_z\rangle=|np(m=0)\rangle,$$

$$|np_x\rangle=\frac{1}{\sqrt{2}}\left[|np(m=1)\rangle-|np(m=-1)\rangle\right],$$

$$|np_y\rangle=\frac{1}{\sqrt{2}}\left[|np(m=1)\rangle+|np(m=-1)\rangle\right],$$

(2)

where np_x, np_y, and np_z orbitals are aligned along the x, y, and z axis, respectively. The np_x orbital is symmetric and the np_y orbital is antisymmetric with respect to the collision plane. The energies and widths of the degenerate states are not affected by the transformation:

$$E_{p_x}=E_{p_y}=E_{np(|m|=1)}; \quad \Gamma_{p_x}=\Gamma_{p_y}=\Gamma_{np(|m|=1)}. \quad (3)$$

From the angular distributions $|\sigma_{np(|m|=1)}(\theta,Z)|^2$ of the $np(|m|=1)$ orbitals, we can obtain the angular distributions for the symmetry-adapted states (see the Appendix):

$$|\sigma_{np(|m|=1)}(\theta,Z)|^2 \Rightarrow \begin{cases} |\sigma_{p_x}(\theta,\varphi,Z)|^2, \\ |\sigma_{p_y}(\theta,\varphi,Z)|^2. \end{cases} \quad (4)$$

In (3) and (4), $E_{np(|m|=1)}$, $\Gamma_{np(|m|=1)}$, and $|\sigma_{np(|m|=1)}(\theta,Z)|^2$ are the results of the static CAM calculation for the $np(|m|=1)$ orbitals, presented in Sec. II B. Using the same notations we can write for the ns and np_z orbitals

$$E_{ns}, \quad \Gamma_{ns}, \quad |\sigma_{ns}(\theta,Z)|^2,$$

$$E_{np_z}=E_{np(m=0)}, \quad \Gamma_{np_z}=\Gamma_{np(m=0)}, \quad (5)$$

$$|\sigma_{np_z}(\theta,Z)|^2=|\sigma_{np(m=0)}(\theta,Z)|^2.$$

B. Rate equation approach for the population evolution

For grazing ion-surface collisions or large temperatures, a rate-equation approach can be used to describe the evolution of the charge state of the scattered particle.[31,38] Taking into account all involved states one can write

$$\frac{dP_j}{dt}=-G_j^l P_j+G_j^c P_{\text{ion}},$$

$$\frac{dP_{\text{ion}}}{dt}=-\left\{\sum_j G_j^c\right\}P_{\text{ion}}+\sum_j G_j^l P_j. \quad (6)$$

In Eq. (6), P_j are the occupations of the alkali-metal-atom orbitals, where $j=\{ns,np_x,np_y,np_z\}$ and P_{ion} is the population of the alkali-metal ion. G_j^l and G_j^c are the electron loss and electron capture rates, respectively. For an Al surface (work function $W\approx4.3$ eV) populations of states differ-

ent from the ground, first excited, and alkali-metal ion state are negligible[29] and the normalization $P_{\text{ion}}+\Sigma_j P_j=1$ holds to a high level of accuracy.

The effect of the parallel velocity ($\mathbf{v}_\parallel$) is incorporated into the theoretical description by taking into account the frame transformation between the ion and the metal.[9,10] In the rest frame of the ion the resonant transition rates are obtained from ($\theta,\varphi=$polar coordinates of the metal-state wave vector $\mathbf{k}$ with respect to the quantization axis):

$$\begin{Bmatrix} G_j^c(Z) \\ G_j^l(Z) \end{Bmatrix} = \Gamma_j(Z) \begin{Bmatrix} g_c \\ g_l \end{Bmatrix} \times \int_0^{\pi/2} \sin\theta \, d\theta \int_0^{2\pi} d\varphi |\sigma_j(\theta,\varphi,Z)|^2$$

$$\times \begin{Bmatrix} f\left(E_F - \dfrac{(\mathbf{k}_j+\mathbf{v}_\parallel)^2}{2}\right) \\ 1-f\left(E_F - \dfrac{(\mathbf{k}_j+\mathbf{v}_\parallel)^2}{2}\right) \end{Bmatrix}, \quad (7)$$

where $g_c=2$ and $g_l=1$ are the spin statistical factors for electron capture and loss, respectively.[5] The angular distributions are normalized as

$$\int_0^{\pi/2} \sin\theta \, d\theta \int_0^{2\pi} d\varphi |\sigma_j(\theta,\varphi,Z)|^2=1. \quad (8)$$

Note, that for ns and np_z orbitals the angle φ in angular distribution is a dummy parameter. $f(E_F-[(\mathbf{k}_j+\mathbf{v}_\parallel)^2/2])$ is the ''Fermi-Dirac'' function ($E_F=$Fermi energy) in the rest frame of the moving ion. It is affected in a characteristic way by the motion parallel to the surface (''shifted Fermi sphere'' model) and can be expressed by the step function ($\mathbf{v}_\parallel$ along the x axis)

$$f\left(E_F - \frac{(\mathbf{k}_j+\mathbf{v}_\parallel)^2}{2}\right) = \Theta\left(E_F - \frac{k_j^2+v_\parallel^2}{2} - v_\parallel k_j \sin\theta\cos\varphi\right), \quad (9)$$

where $k_j\equiv|\mathbf{k}_j|$ is fixed by the resonance condition: $k_j = \sqrt{2(E_F+W+E_j)}$ with the modified energies E_j of alkali-metal atom orbitals in front of the Al surface as presented in Fig. 1(a).

The motion parallel to the surface breaks the degeneracy of the np_x and np_y orbitals with respect to the capture and loss rates. This is a direct consequence of Eq. (7) and the difference in angular distributions for those orbitals.

IV. EXPERIMENTAL CONSIDERATIONS

The measurements of charge fractions in the scattered beams appear as a simple problem at first glance. However, experiments under grazing angles of incidence probe large lateral extensions of the target so that the ''quality'' of the target surface plays an essential role. A simple measure of that ''quality,'' i.e., a surface widely free from adsorbates and low densities of steps, is the angular broadening of the scattered beams, which has been shown to be gradually reduced in the experiments in recent years. The neutral fractions are found to depend on the surface defect structure, so that for an adequate comparison with our theoretical studies surfaces prepared with great care are essential experimental prerequisites. In this respect early studies, such as, e.g., those

reported in Ref. 5, provided data that are possibly slightly affected by a binary type of collisions with atoms forming defect structure. This has to be considered in quantitative comparisons with theory.

All data presented here for Li and Na stem from recent measurements with improved experimental conditions, i.e., base pressure in an UHV chamber of about 2×10^{-11} mbar, well-defined scattered beams with an angular broadening of some 0.1° only, and average terrace widths on the Al(111) sample of larger than about 50 nm with a clear dominance of monatomic step heights. Furthermore, attention is paid to the effect of the image charge interaction on the trajectory of ions. This interaction causes a slight angular shift between the angular distributions for neutral atoms and ions and has to be taken into account for a reliable analysis with respect to charge fractions. In particular, at very small angles of incidence ($<0.5°$) this feature causes substantial problems in the analysis of charge fractions.

V. RESULTS AND DISCUSSION

Populations of different orbitals and total neutral fractions in the scattered beam,

$$N_{\text{neut}}=\sum_j P_j, \quad (10)$$

are obtained by the numerical integration of Eq. (6) on the outgoing path of the straight-line trajectory of the scattered particle. The starting point of the integration Z_{ini} is chosen in such a way that the final results do not depend on the initial conditions for the populations imposed at Z_{ini} (typically $Z_{\text{ini}}\approx3$ a.u. from the image reference plane). Indeed, close to the surface the resonant charge-transfer process is very fast. Any memory of the initial populations is quickly erased and the system relaxes towards a local equilibrium population given by the competition between loss and capture rates in Eq. (6). Distances important for the final charge-state formation (''freezing distance'' concept[30]) are rather large (≈10–11 a.u.) in the present case.

A. Na⁺ neutralization at an Al(111) surface

In Fig. 3 we present the results for the Na$^+$ neutralization in grazing scattering from an Al surface. Exit angle is 0.5° with respect to the surface plane and work function is $W=4.29$ eV as actually measured via photoemission.[39] For small $v_\parallel$, sodium ions are neutralized completely into the Na($3s$) ground state. When the parallel velocity is increased, the fraction of the neutral particles decreases following the ground-state population evolution. Starting from $v_\parallel\approx0.15$ a.u. the excited Na($3p$) state is populated and the total population of neutral atoms is shared between Na($3s$) and Na($3p$) states. The dashed-dotted line in Fig. 3 presents the total population of the excited atoms:

$$N_{\text{exc}}=P_{p_x}+P_{p_y}+P_{p_z}. \quad (11)$$

As a function of the parallel velocity the Na($3p$) population has a resonant shape with a maximum at $v_\parallel\approx0.425$ a.u. This is clearly different from the dependence of the ground-state population on $v_\parallel$. The origin of this difference lies in the
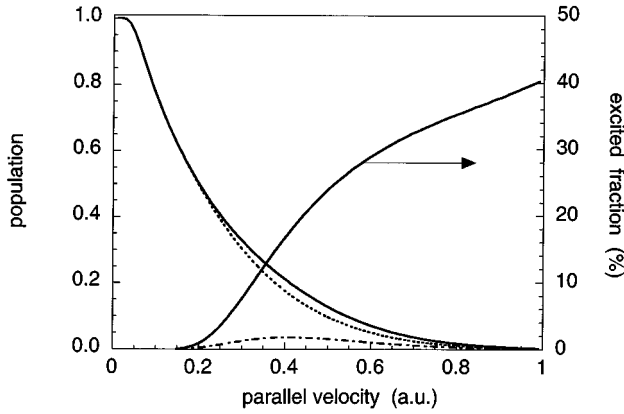
FIG. 3. Population of neutral atoms formed in grazing scattering of Na$^+$ ions at Al(111) surface as a function of the velocity component parallel to the surface. Exit angle is 0.5° with respect to the surface plane, work function $W = 4.29$ eV. Solid line, total neutral fraction; short dashed line, Na(3s)-state population; dashed-dotted line, Na(3p)-state population. The solid line with an arrow represents the fraction of excited atoms in the neutral population.

different energies of the $3s$ and $3p_{x,y,z}$ orbitals with respect to the Fermi level at atom-surface distances relevant for the final charge-state formation. Indeed at these distances ($Z \approx 10$–11 a.u.), the $3s$ orbital is in resonance with occupied electronic states of the metal below the Fermi level, whereas the $3p_{x,y,z}$ orbitals are in resonance with unoccupied electronic states of the metal above the Fermi level. According to the ''shifted Fermi sphere'' model,[5] this leads to the two different parallel velocity dependences of the orbital populations. It follows from our results (Fig. 3) that the total excited fraction of the neutral particles in the scattered beam,

$$\Omega_{\text{exc}} = \frac{N_{\text{exc}}}{N_{\text{neut}}}, \qquad (12)$$

increases with increasing $v_\parallel$ and reaches 40% for $v_\parallel = 1$ a.u.

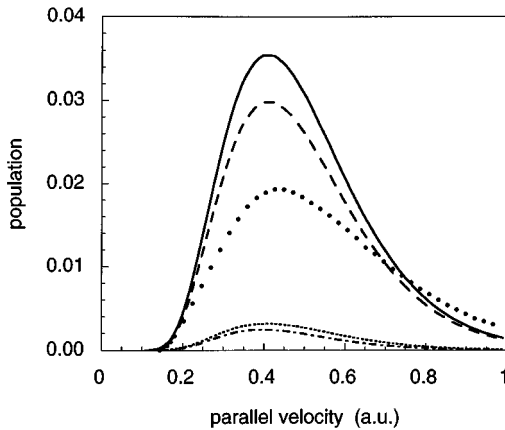In Fig. 4 we present the results for the populations of the

FIG. 4. Total Na(3p)-state population (solid line) and its sharing between $3p_x$ (long dashed line), $3p_y$ (short dashed line), and $3p_z$ (dashed-dotted line) orbitals. Also for comparison Na(3p)-state population extracted from the experimental results in Ref. 29 is presented (black dots). Scattering conditions are described in the caption for Fig. 3.

various Na(3p) substates. Also for comparison we present the total Na(3p) population deduced from experimental data.[29] Experimental and theoretical results are in good agreement with respect to the parallel velocity threshold and maximum of the Na(3p) formation. Our calculation predicts $\approx 3.6\%$ for the maximum fraction of excited states in the scattered beam which compares well (taking into account the uncertainties in the analysis of Ref. 29) to the $\approx 2\%$ deduced from the experiment. As it is seen in Fig. 4, the population of the $3p_x$ orbital is one order of magnitude larger than that of the $3p_y$ and $3p_z$ orbitals. This results from the φ dependence of the angular distribution of this orbital which produces a strong coupling to the occupied metal states.

Our results on the population of different substrates of the Na(3p) state have a direct consequence on the polarization of the emitted light. Indeed, the propensity for populating the atomic $3p_x$ orbital aligned along the beam direction over the p_z orbital aligned along the surface normal agrees with the experimental and theoretical findings on the light polarization in grazing scattering from metal surfaces.[25–28] As well, we find a propensity for populating the $3p_x$ over the $3p_y$ orbital oriented normal to the scattering plane. From our results we conclude that subsequent light emission along both the surface normal and perpendicular to the scattering plane should be preferentially polarized linearly along the beam direction.

In Fig. 5 we compare calculated neutral fractions in the scattered beam with experimental results for three different values of the normal velocity component. Calculation is performed for the work function $W = 4.29$ eV measured experimentally.[39] We find excellent agreement between theory and experiment over the whole $v_\parallel$ range where experimental data are available.

B. K$^+$ neutralization at an Al(111) surface

Theoretical and experimental[5] results for K$^+$ neutralization at an Al(111) surface are compared in Fig. 6 for an exit angle of the scattered particles of 0.7° with respect to the surface plane. Work-function measurements were not performed in Ref. 5. Therefore the calculations were performed for the three different values of the work function which can be found in the literature for an Al(111) surface: $W = 4.29$, 4.27, and 4.25 eV. As one can see from Fig. 6, the differences in K-neutral fractions obtained for different work functions are small. The differences vanish for larger parallel velocities, when kinematically induced transformation of the Fermi-Dirac distribution is more important than the differences in W. As for Na projectiles, a very good agreement between theory and experiment is obtained.

In Fig. 7 we present the results for the population sharing between the K(4s) and K(4p) states. Compared to the Na case, larger fractions of neutrals are in the excited K(4p) state above the kinematic threshold. Note that ground-state and total neutral population depend on $v_\parallel$ in a completely different way than for Na. In fact, the K(4s) ionization potential is smaller compared to Na(3s). As shown in Fig. 1(a), already at large atom-surface distances the K(4s) level is shifted by the image charge interaction above the Fermi level into resonance with unoccupied metal states. As a result, 4s-orbital population has the ''resonant-type'' of $v_\parallel$ dependence (see also discussion in Ref. 5). The K(4p) formation
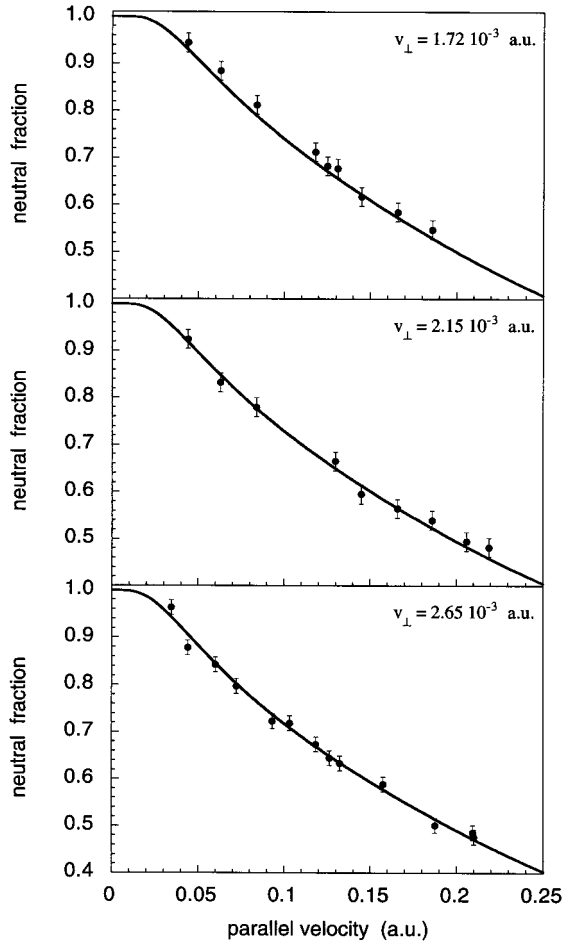
FIG. 5. Comparison between experimental (black dots with error bars) and theoretical results (solid line) for the sodium neutral fractions formed in grazing scattering at Al(111) surface. Results are presented for three different values of the velocity component normal to the surface, as functions of the velocity component parallel to the surface.

threshold is at larger $v_{\parallel}$ than that for the ground state due to its smaller ionization potential.

Details on the population sharing between the $4p_x$, $4p_y$, and $4p_z$ orbitals are presented in Fig. 8. In absolute numbers less excited states are formed, compared to Na scattering from Al. This is a direct consequence of the larger energy gap between the Fermi level and K($4p$) sublevels. Basically, the decrease of the ionization potential by ≈ 0.31 eV [from 3.04 eV for Na($3p$) to 2.73 eV for K($4p$)] leads to the decrease of the excited state population by a factor of 2. For the populations of $4p_x$, $4p_y$, and $4p_z$ orbitals, the same feature as for Na are found: the p_x orbital is populated an order of magnitude more efficiently than the p_y and p_z orbitals.

C. Li$^+$ neutralization at Al(111) surface

In Fig. 9 we present the calculated Li neutral fractions in the outgoing beam for the grazing scattering with a fixed normal velocity value ($v_{\perp} = 3.33 \times 10^{-3}$ a.u.) and compare them to the experimental results. We present also the results for the population shared between the ground Li($2s$) and excited Li($2p$) states. The work function $W = 4.27$ eV cor-
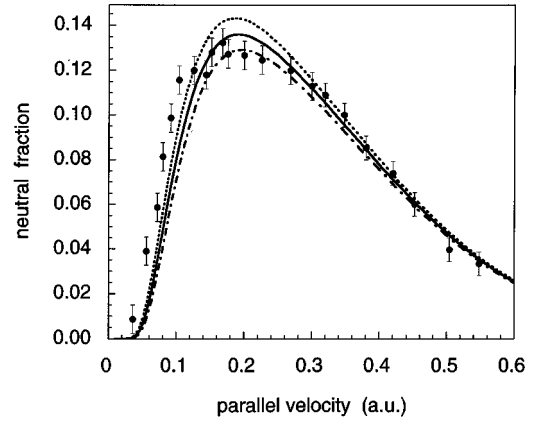

FIG. 6. Potassium neutral fraction formed in grazing scattering at Al(111) surface as a function of the velocity component parallel to the surface. The exit angle is 0.7° with respect to the surface plane. Experimental results are presented by the black dots with error bars. The calculation has been performed for three different work functions: 4.25 eV (short dashed line), 4.27 eV (solid line), and 4.29 eV (dashed-dotted line).

responds to the one measured experimentally. Agreement between experimental and theoretical results is rather satisfactory except for higher $v_{\parallel}$. When judging this deviation one has to take into account that those experimental data correspond to rather small exit angles where the analysis of neutral fractions is a problem due to surface imperfections and image charge effects.[39]

The Li ground state lies below the Fermi level, except for very small atom-surface distances, which are not important for the final charge-state formation. Therefore, the total neutral fraction in the scattered beam and ground-state population have the same dependence on parallel velocity as was observed for Na. A peculiarity of Li$^+$ scattering from Al is an essential fraction of excited particles in the scattered beam above the kinematic threshold for Li($2p$) formation. At the maximum for the Li($2p$) formation, 12% of the scattered
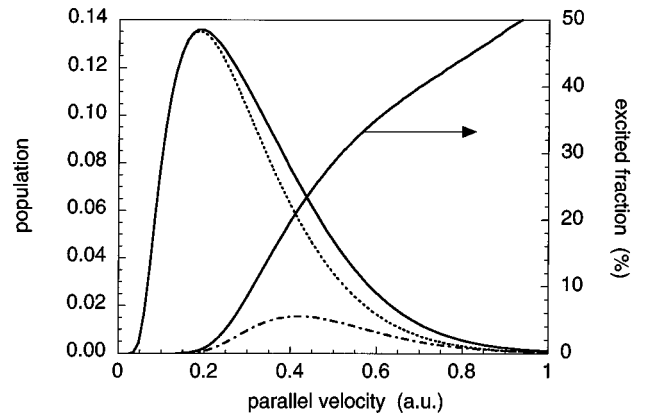

FIG. 7. Population of neutral atoms formed in grazing scattering of K$^+$ ions at Al(111) surface as a function of the velocity component parallel to the surface. The exit angle is 0.7° with respect to the surface plane, and the work function $W = 4.27$ eV. Solid line, total neutral fraction; short dashed line, K($4s$)-state population; dashed-dotted line, K($4p$)-state population. The solid line with an arrow represents the fraction of excited atoms in the neutral population.
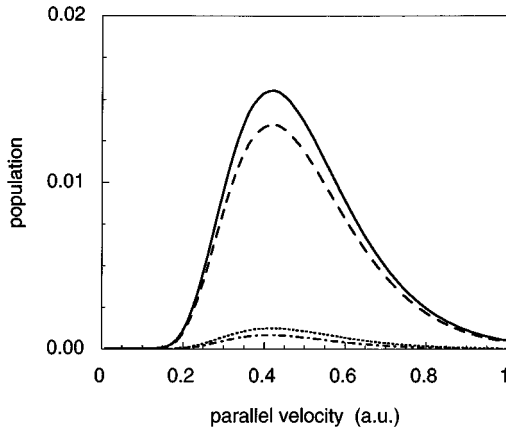
FIG. 8. Total K(4p)-state population (solid line) and its sharing between 4p_x (long dashed line), 4p_y (short dashed line), and 4p_z (dashed-dotted line) orbitals. Scattering conditions are described in the caption for Fig. 7.

particles are in an excited state compared, e.g., to 3.6% for Na(3p). At $v_{\parallel}=1$ a.u., 60% of the neutral particles scattered from the surface are excited. This is due to the relative proximity of the energies of the Li(2p) substates to the Fermi level of Al. Populations shared between different excited orbitals have the same features as discussed in Secs. V A and V B.

VI. SUMMARY AND CONCLUSIONS

We have performed a theoretical study of alkali-metal ion neutralization in grazing scattering from an Al(111) surface. Total neutral fractions in the scattered beam were obtained as functions of the scattering conditions. Populations of the ground state as well as of the first excited states were calculated together with the populations of the np_x-, np_y-, and np_z-excited sublevels. The populations of the states have two different types of $v_{\parallel}$ behavior: (i) monotonic decrease with increasing $v_{\parallel}$ [Na(3s)-like]; (ii) resonant shape [Na(3p)-like]. This can be understood from the ''shifted Fermi sphere'' model by taking into account the energies of the different orbitals with respect to the Fermi energy. We summarize the characteristic results in Table I.

Since ground-state populations dominate over the excited state populations in a wide range of $v_{\parallel}$ (except for very large $v_{\parallel}$), the total neutral fraction dependence on $v_{\parallel}$ is given by that of the ground state.

The excited-state degeneracy is lifted due to the surface potential and parallel motion. Three orbitals are formed
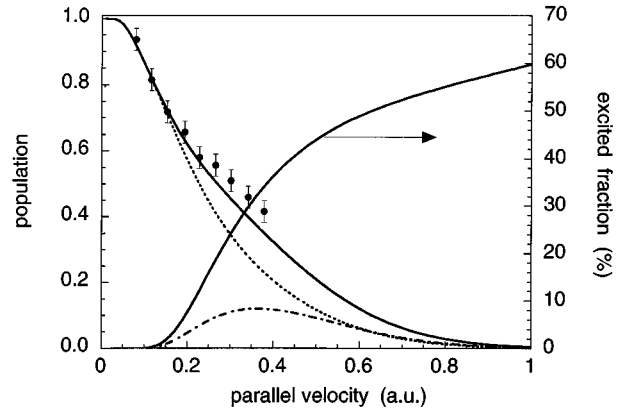

FIG. 9. Comparison between experimental and theoretical results for the Li$^+$ neutralization in grazing scattering at Al(111) surface for a fixed normal velocity ($v_{\perp}=3.33\times10^{-3}$ a.u.) as a function of the velocity component parallel to the surface. Experimentally measured neutral fractions are represented by the black dots with error bars. The solid line presents the calculated total neutral fraction: short dashed line, Li(2s)-state population; dashed-dotted line, Li(2p)-state population. The solid line with an arrow represents the fraction of the excited atoms in the neutral population. Calculations are performed for the work function $W=4.27$ eV.

(np_x, np_y, and np_z) having different properties with respect to the charge-exchange process. We find the np_x orbital oriented along the beam direction to be populated by an order of magnitude more efficiently than the np_y and np_z orbitals. This has direct consequences on the polarization of the emitted light in agreement with experimental observations.

Finally we point out that the total neutral fractions in the scattered beams, obtained with our nonperturbative and parameter-free study, agree with experimental results on a quantitative level.

APPENDIX

In this appendix we discuss how the angular distributions can be obtained for the symmetry-adapted basis. The ''static'' CAM calculation uses the cylindrical symmetry of the problem with respect to the surface normal going through the atom center. The active electron wave function is expanded over spherical harmonics $Y_{lm}(\theta,\varphi)$, where m is fixed and given by the projection of the angular momentum of the electron on the quantization z axis.[15] The angular distribution is obtained from the eigenvector $Q_{|m|}$ of the time-delay matrix:[11]

TABLE I. Schematic behavior of the alkali/Al(111) charge transfer.

State	$|E_j(\infty)|$	$\dfrac{|E_j(\infty)|-W}{\text{''freezing distance'' region}}$	$v_{\parallel}$ dependence	Population maximum
Li(2s)	5.39 eV	>0	Na(3s)-like	1
Li(2p) manifold	3.54 eV	<0	Na(3p)-like	0.12
Na(3s)	5.14 eV	>0	Na(3s)-like	1
Na(3p) manifold	3.04 eV	<0	Na(3p)-like	0.036
K(4s)	4.34 eV	<0	Na(3p)-like	0.14
K(4p) manifold	2.73 eV	<0	Na(3p)-like	0.016

$$|\sigma_i(\theta,Z)|^2 = \left| \sum_l Q_{l|m|}^i(Z) Y_{lm}(\theta,\varphi) \right|^2, \qquad \text{(A1)}$$

where $i = \{ns, np(m=0), np(|m|=1)\}$. Because of the cylindrical symmetry the results for $m=1$ and -1 are degenerate. $|\sigma_i(\theta,Z)|^2$ does not depend on the φ angle. Indeed,[40]

$$Y_{lm}(\theta,\varphi) = (-1)^{(m+|m|)/2} C_{l|m|} P_l^{|m|}(\cos\theta) e^{im\varphi}, \quad \text{(A2)}$$

where $C_{l|m|}$ are the normalization constants and $P_l^{|m|}(\cos\theta)$ are the Legendre polynomials. Substitution of Eqs. (A2) into (A1) removes any φ dependence.

In the present work we have to make a transformation from a basis set with a given m to a basis set with given symmetry with respect to the (x,z) plane. If the active electron is associated to $m=0$, it corresponds to a symmetric wave function and no transformation is required [see Eq. (5) in the text]. The case of $|m|=1$ electrons requires a transformation. $Y_{l1}(\theta,\varphi)$ and $Y_{l-1}(\theta,\varphi)$ states can be mixed in the following way to form symmetric and antisymmetric wave functions:

$$F^s(\theta,\varphi) = \frac{1}{\sqrt{2}} [Y_{l1}(\theta,\varphi) - Y_{l-1}(\theta,\varphi)],$$

$$\text{(A3)}$$

$$F^a(\theta,\varphi) = \frac{1}{\sqrt{2}} [Y_{l1}(\theta,\varphi) + Y_{l-1}(\theta,\varphi)].$$

The angular distribution obtained as Eq. (A1) in fact comes from a static calculation with a given m, i.e., this angular distribution is implicitly associated with an $e^{i\varphi}$ or $e^{-i\varphi}$. Thus, similarly with Eqs. (A3), one can form the angular distributions for the symmetric and antisymmetric components as

$$|\sigma_{np_x}(\theta,\varphi,Z)|^2 = \frac{1}{2} \left| \sum_l Q_{l1}^{np(|m|=1)}(Z) [Y_{l1}(\theta,\varphi) - Y_{l-1}(\theta,\varphi)] \right|^2,$$

$$\text{(A4)}$$

$$|\sigma_{np_y}(\theta,\varphi,Z)|^2 = \frac{1}{2} \left| \sum_l Q_{l1}^{np(|m|=1)}(Z) [Y_{l1}(\theta,\varphi) + Y_{l-1}(\theta,\varphi)] \right|^2.$$

From Eqs. (A4), (A1), and (A2) we finally obtain

$$|\sigma_{np_x}(\theta,\varphi,Z)|^2 = 2|\sigma_{np(|m|=1)}(\theta,Z)|^2 \cos^2\varphi,$$

$$\text{(A5)}$$

$$|\sigma_{np_y}(\theta,\varphi,Z)|^2 = 2|\sigma_{np(|m|=1)}(\theta,Z)|^2 \sin^2\varphi.$$

[1] J. J. C. Geerlings and J. Los, Phys. Rep. **190**, 133 (1990).

[2] R. Brako and D. M. Newns, Rep. Prog. Phys. **52**, 655 (1989).

[3] B. H. Cooper and E. R. Behringer, in *Low Energy Ion-Surface Interactions*, edited by J. W. Rabalais (Wiley, New York, 1994).

[4] H. Winter and R. Zimny, in *Coherence in Atomic Collision Physics*, edited by H. J. Beyer, K. Blum, and R. Hippler (Plenum, New York, 1988); H. Winter, Comments At. Mol. Phys. **26**, 287 (1991).

[5] R. Zimny, H. Nienhaus, and H. Winter, Radiat. Eff. Defects Solids **109**, 9 (1989).

[6] F. Wyputta, R. Zimny, and H. Winter, Nucl. Instrum. Methods **B58**, 379 (1991).

[7] D. R. Bates and R. McCaroll, Proc. R. Soc. London Ser. A **245**, 175 (1958).

[8] T. A. Green, Proc. R. Soc. London **86**, 1017 (1965).

[9] J. N. M. van Wunnik, R. Brako, K. Makoshi, and D. M. Newns, Surf. Sci. **126**, 618 (1983).

[10] D. M. Newns, K. Makoshi, R. Brako, and J. N. M. van Wunnik, Phys. Scr. **T6**, 5 (1983).

[11] A. G. Borisov, D. Teillet-Billy, and J. P. Gauyacq, Phys. Rev. Lett. **68**, 2842 (1992).

[12] J. J. C. Geerlings, P. W. van Amersfoort, L. F. Tz. Kwakman, E. H. A. Granneman, J. Los, and J. P. Gauyacq, Surf. Sci. **157**, 151 (1985).

[13] P. Nordlander and J. C. Tully, Phys. Rev. Lett. **61**, 990 (1988).

[14] P. Nordlander and J. C. Tully, Phys. Rev. B **42**, 5564 (1990).

[15] D. Teillet-Billy and J. P. Gauyacq, Surf. Sci. **239**, 343 (1990).

[16] S. A. Deutscher, X. Yang, and J. Burgdörfer, Nucl. Instrum. Methods **B100**, 336 (1995).

[17] M. C. Desjonqueres and D. Spanjaard, *Concepts in Surface Physics*, Springer Series in Surface Science Vol. 30 (Springer-Verlag, Berlin, 1993).

[18] R. Zimny, Surf. Sci. **260**, 347 (1992).

[19] M. Alducin, F. J. Garcia de Abajo, and P. M. Echenique, Phys. Rev. B **49**, 14 589 (1994).

[20] H. J. Andrä, R. Zimny, H. Winter, and H. Hagedorn, Nucl. Instrum. Methods **B9**, 572 (1985).

[21] N. Tolk, J. C. Tully, J. C. Kraus, W. Heiland, and S. H. Neff, Phys. Rev. Lett. **41**, 643 (1979).

[22] H. Shall, H. Brenten, K. H. Knorr, and V. Kempter, Z. Phys. D **16**, 161 (1990).

[23] D. R. Andersson, E. R. Behringer, B. H. Cooper, and J. B. Marston, J. Vac. Sci. Technol. A **11**, 2133 (1993); D. R. Andersson, E. R. Behringer, B. H. Cooper, C. A. DiRubio, G. A. Kimmel, and C. Richardson, Phys. Rev. B **48**, 7809 (1993).

[24] J. Burgdörfer, E. Kupfer, and H. Gabriel, Phys. Rev. A **35**, 4963 (1987).

[25] C. Marsch and H. Winter, Z. Phys. D **18**, 25 (1991).

[26] R. Brako, Phys. Rev. B **30**, 5629 (1984).

[27] R. Brako, H. Winter, and D. M. Newns, Europhys. Lett. **7**, 213 (1988).

[28] R. Zimny and A. G. Borisov, Z. Phys. D **30**, 225 (1994).

[29] H. Winter, Z. Phys. D **17**, 109 (1990).

[30] E. G. Overbosch, B. Rasser, A. D. Tenner, and J. Los, Surf. Sci. **92**, 310 (1980).

[31] D. C. Langreth and P. Nordlander, Phys. Rev. B **43**, 2541 (1991).

[32] A. G. Borisov, D. Teillet-Billy, and J. P. Gauyacq, Nucl. Instrum. Methods **B78**, 49 (1993).

[33] J. N. Bardsley, Case Studies At. Phys. **4**, 299 (1974).

[34] R. O. Jones, P. J. Jennings, and O. Jepsen, Phys. Rev. B **29**, 6474 (1984).

[35] P. J. Jennings, R. O. Jones, and M. Weinert, Phys. Rev. B **37**, 6113 (1988).

[36] F. J. Garcia de Abajo and P. M. Echenique, Phys. Rev. B **46**, 2663 (1992).

[37] J. F. Anett and P. M. Echenique, Phys. Rev. B **34**, 6853 (1986).

[38] J. J. C. Geerlings, J. Los, J. P. Gauyacq, and N. M. Temme, Surf. Sci. **172**, 257 (1986).

[39] A. G. Borisov, H. Winter, G. Dierkes, and R. Zimny, Europhys. Lett. **33**, 229 (1996).

[40] A. Messiah, *Mecanique Quantique* (Dunod, Paris, 1995), Tome 1, App. B.